

# Residual stresses in wire-arc additive manufacturing – Hierarchy of influential variables

Q. Wu<sup>a,b</sup>, T. Mukherjee<sup>b</sup>, A. De<sup>c</sup>, T. DebRoy<sup>b,\*</sup>

<sup>a</sup> School of Mechanical Engineering, Beijing Institute of Technology, Beijing 100081, China

<sup>b</sup> Department of Materials Science and Engineering, The Pennsylvania State University, University Park, PA 16802, USA

<sup>c</sup> Department of Mechanical Engineering, IIT Bombay, Powai, Mumbai 400076, India

## ARTICLE INFO

### Keywords:

Wire-arc additive manufacturing  
Residual stresses  
Machine learning  
Neural network  
Random forest  
Delamination

## ABSTRACT

Residual stresses and distortion are common serious defects in wire-arc additive manufacturing. Commercial thermomechanical models are often used to understand how these defects form. However, no clear mitigation strategy has evolved from previous research. Identification of the hierarchy of variables that influence residual stresses will help to uncover practical means of mitigating this difficulty. Here we use multiple machine learning algorithms and a mechanistic model to rank separately both easy to measure process parameters as well as thermomechanical variables that affect the evolution of stresses. We analyze 243 sets of residual stress data for three alloys using random forest and neural network algorithms to uncover the relative influences of the variables. Both these algorithms predict residual stresses with 97 % accuracy. More important, both algorithms provide the same hierarchical influence of process variables on stresses. The substrate preheat temperature is the most influential variable among the process variables. Among the thermomechanical variables, the following variables are the most influential in decreasing order of importance: the gap between the solidus and preheat temperatures, the product of elastic modulus and the coefficient of thermal expansion, molten pool volume, substrate rigidity, and heat input.

## 1. Introduction

Wire-arc additive manufacturing (WAAM) is widely used because of its high deposition rate and low cost [1–3]. However, shrinkage of large pools of liquids during solidification and repeated heating and cooling result in high residual stresses [1] and defects such as delamination, warping, buckling and dimensional inaccuracy [4–7]. Many simultaneously occurring physical processes affect the evolution of residual stresses in the components. The resulting complexity of the process precludes any straightforward determination of variables that could be adjusted to reduce stresses and mitigate defects.

The effects of individual variables on the accumulation of residual stresses have been investigated in several variants of AM. For example, preheating of the substrates is known to reduce residual stresses and distortions in WAAM [8]. A decrease in laser power was found to reduce residual stresses in components fabricated by both directed energy deposition (DED) [9] and powder bed fusion (PBF) [10]. Besides, residual stresses along the scanning direction are decreased by increasing scanning speed during PBF [11]. Thicker substrates are thought to increase residual stresses at the substrate-deposit interface [12].

However, the aforementioned results do not identify the most important variables that influence the evolution of residual stresses. The roles of individual variables on the evolution of stresses in a multi-variable process are often masked by the impacts of other variables and the complexity of the process. As a result, it is difficult to uncover the hierarchy of the important variables.

Data-driven machine learning techniques are often beneficial to establish relations among different sets of variables when phenomenological relations among them are unavailable. Machine learning (ML) methods have been used to predict stresses in the related field of welding [13,14]. Both neural networks and neuro-fuzzy system models have been used to predict residual stress distribution in pipe welds. The performances of the two machine learning models have also been compared [13]. It was also shown that the artificial neural network and multi-objective optimization algorithms helped to reduce the residual stresses and distortion in welding [15]. The application of support vector regression and neuro-evolutionary computing were also used in welding [16,17] based on data calculated from the finite element models. Probabilistic kernel machine models were tested on experimentally-obtained data of axial and hoop residual stresses in two

\* Corresponding author.

E-mail address: [debroy@psu.edu](mailto:debroy@psu.edu) (T. DebRoy).

<https://doi.org/10.1016/j.addma.2020.101355>

Received 6 March 2020; Received in revised form 15 May 2020; Accepted 21 May 2020

Available online 30 May 2020

2214-8604/ © 2020 Elsevier B.V. All rights reserved.

stainless-steel pipes [18]. These examples indicate the effectiveness of applying machine learning methods to predict residual stresses in welding. However, there is a scarcity of literature in predicting stresses in WAAM using machine learning methods. What is needed and not currently available is a data-driven analysis of residual stresses in WAAM to evaluate the hierarchy of the most important factors that affect residual stresses.

Here, for the first time, we analyze data on residual stresses during various conditions of WAAM using data-driven machine learning. Two hundred and forty-three sets of data on residual stresses for single layer deposits of three alloys, IN 718, SS 316 and 800H are analyzed. In the appendix, we justify in detail why we consider the results of single layer deposits for machine learning. First, hierarchical influences of easy to measure WAAM variables such as arc power, scanning speed, substrate preheat temperature, and substrate thickness, as well as alloy properties, e.g., yield stress, coefficient of thermal expansion, thermal diffusivity and Young's modulus on residual stresses, are investigated. However, these process parameters are distributed over a very large range where the effects of individual variables are concealed by the complexity of the thermomechanical behavior of the system. There are complex thermomechanical variables that are better representatives of the complex evolution mechanism of residual stresses. The use of several complex variables that cannot be easily measured compared to the individual process variables is well-recognized in the fluid flow through a pipe. The variables such as the diameter of the pipe, average velocity, density and viscosity of the fluid can determine whether the flow in a pipe is turbulent or laminar. However, the flow behavior is much better showed by the Reynolds number than the four individual variables. Therefore, here we separately identify five complex thermomechanical variables that influence residual stresses and delamination. They include three thermal variables, the difference between solidus and preheat temperature, liquid pool volume, heat input, and mechanical variables, substrate rigidity, and the product of elastic modulus and coefficient of thermal expansion.

The residual stresses are obtained using a well-tested commercial thermomechanical model. A neural network and a random forest-based machine learning algorithms are selected to predict their hierarchical influences of variables that affect residual stresses. Neural network algorithms have a strong ability to recognize the underlying complex relationships between input variables and the responses [19,20]. Also, a random forest algorithm works well with different types of input variables and is good at handling non-linear parameters efficiently [21]. Although we investigate residual stresses in WAAM of three alloys, it is equally applicable for other alloys and AM variants.

## 2. Methods

The methodology for this research is shown schematically in Fig. 1. Two types of datasets are used in machine learning as inputs. First, the raw, unprocessed WAAM variables that are easy to measure and record during the experiments and simple alloy properties are used. Second, the causative variables that represent complicated thermomechanical behavior of the system are calculated using a well-tested, thermomechanical model and used in machine learning. The residual stresses calculated by the thermomechanical model are used as the outputs of machine learning. The details of the thermomechanical model, data generation method and machine learning (ML) algorithms are described below.

### 2.1. Thermomechanical model

A finite element method based thermomechanical model is used to calculate 3D, transient temperature and residual stresses distributions. The calculation procedures have been described in detail in our previous publication [4] and are not repeated here. Only a few salient features of the model are described here. The solution domain for the thermomechanical calculations consisting of the substrate and a single-layer and a single-hatch deposit is shown in Fig. 2. First, temperature fields are computed by solving the heat conduction equation [22] where the heat input is applied as a double ellipsoidal heat source [4]. The heat losses by convection and radiation from the surfaces of the deposit and substrate are applied as boundary conditions. Temperature-dependent thermophysical and mechanical properties of the alloys used in the calculations are provided in the supplementary document. 3D distribution of residual stresses is calculated based on the transient temperature field [23]. During the deposition, the components are clamped at four corners to resist movement which is simulated by fixing the nodes at the four corners on the top surface of the deposit as shown in Fig. 2. When the components cool down to the room temperature, the clamps are released by deactivating the restriction of the nodes at the four corners. A commercial software, Abaqus, is used for these calculations [24].

### 2.2. Generation of datasets

Residual stresses have three primary components along x, y and z axes. Besides, all three components are spatially non-uniform. Therefore, to figure out which component of residual stresses and at what location should be considered to generate the database for ML, all three components are compared. Fig. 3 compares the three components of residual stress distributions of an IN 718 part. For all three components, very high tensile stress is observed near the substrate-deposit interface. In Fig. 3 (d), all three components are plotted along line 1 (see Fig. 2) which is near the substrate-deposit interface. The stress component along y-direction (scanning direction) which is also called the longitudinal stress is the highest among the three components. This is primarily because the deposit mainly shrinks along the scanning direction during cooling [25,26]. From Fig. 3 (d), it can also be found that the longitudinal stress at the substrate-deposit interface is almost constant. Therefore, longitudinal stresses (y-direction) at the center of the substrate-deposit interface (Point 'A' in Fig. 2) are used to generate the database for ML. This value of residual stress is also responsible for delamination in WAAM [4,23].

The residual stresses in WAAM are influenced by process parameters such as arc power, scanning speed, substrate preheat temperature and substrate thickness as well as alloy properties [1]. Therefore, these four aforementioned process parameters are varied for three commonly used alloys, IN 718, SS 316 and 800H to generate the database for ML. For each of the four process parameters, three different levels are selected within the commonly used range in WAAM. Therefore, there are  $3^4$  i.e. 81 cases for each of the three alloys which generate 243 data points as input for machine learning. The ranges of the process parameters and alloy properties are provided in Table 1. Causative variables calculated using the thermomechanical model corresponding to the 243 cases are also used as inputs to machine learning. The ranges of the causative variables are also provided in Table 1. The output variable of the machine learning is longitudinal residual stress at the mid-length of the deposit near the substrate-deposit interface. For both the raw process

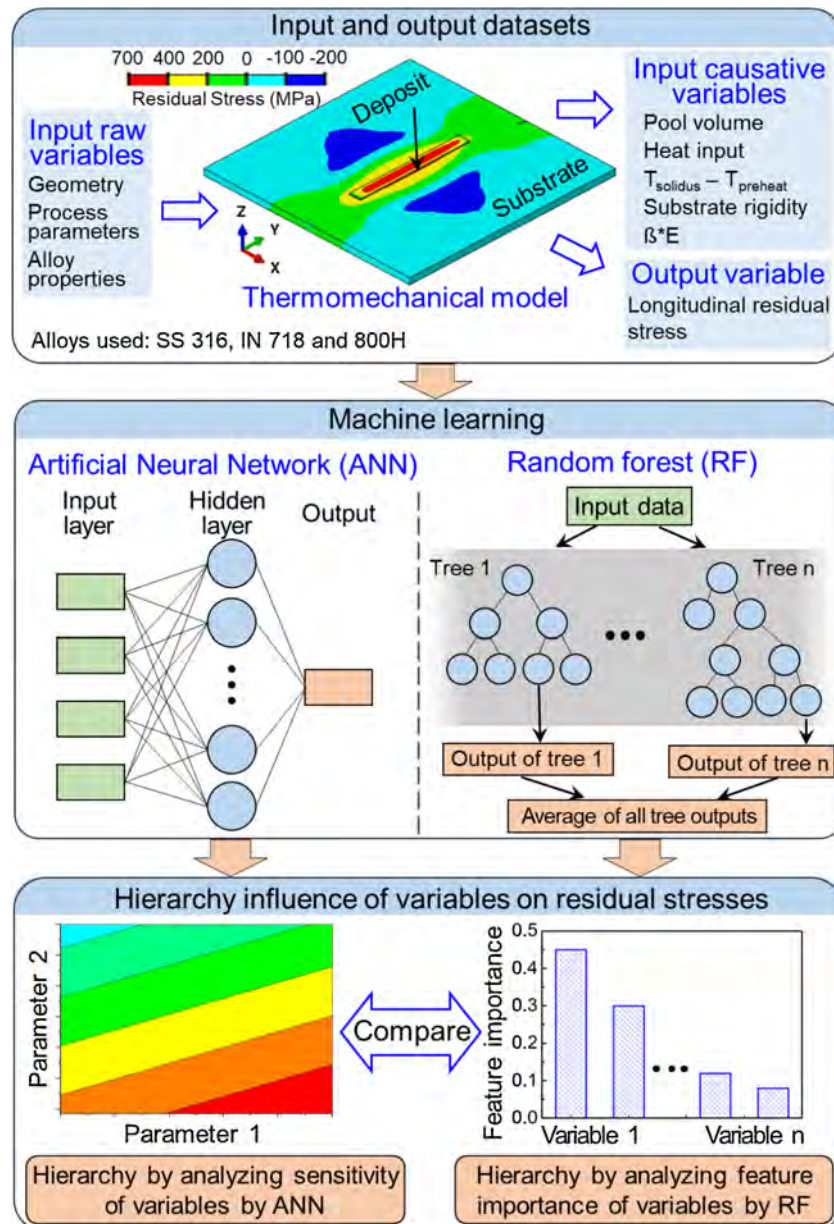


Fig. 1. Schematic representation of the methodology used in this research. The symbol  $\beta$  represents the coefficient of thermal expansion and E is the Young's Modulus.

variables and causative variables, 80 % of the total of 243 data points (i.e. 194 data points) are randomly selected for training and the remaining 20 % (i.e. 49 data points) are used for testing. The random selection process is repeated five times and the accuracy reported in this work is the average accuracy of these five trials.

### 2.3. Machine learning algorithms

Two machine learning algorithms, artificial neural networks (ANN) and random forests (RF) are used in this work. For the ANN algorithm, the number of hidden layers, nodes in each hidden layer and the activation function are the critical factors [27]. The randomized search method [28] is used to find the optimum combination of these factors

that provides the best accuracy. In this work, two hidden layers with 32 nodes in each layer and the ReLU activation function [29] are found to be the optimum combination. RF algorithm creates multiple decision trees as subsets and combines the outputs of them, which can help to reduce the overfitting of the dataset [30]. Also, RF is good for providing a feature-based ranking of variables [31]. In this work, the ranking of variables is performed by calculating the feature importance of variables which is defined as the total decrease in node impurity averaged over all trees of the random forest [32]. Therefore, feature importance is an indicator that can evaluate the relative importance of the input variables on the desired outputs. The larger is the feature importance, the more important is the variable to the output. An open-source Python package “Sci-kit learn” was used in this work to implement both

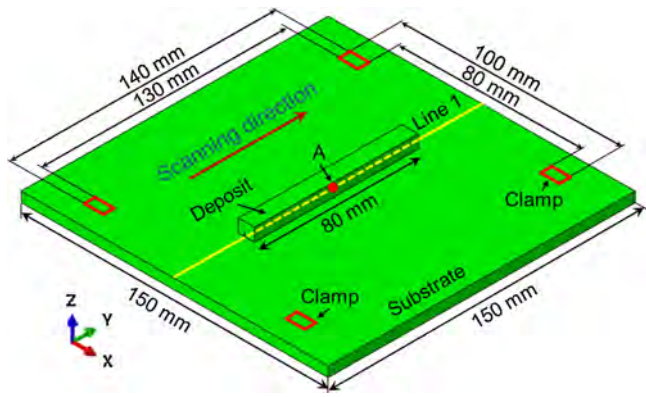


**Fig. 2.** Schematic representation of the solution domain of the thermo-mechanical model. Line 1 represents the substrate-deposit interface at the mid-width of the deposit. The point ‘A’ is at the mid-length, mid-width of the deposit. Deposit and substrate dimensions are indicated in the figure. Substrate thickness is a variable input as indicated in Table 1. Scanning direction is along the positive Y-axis.

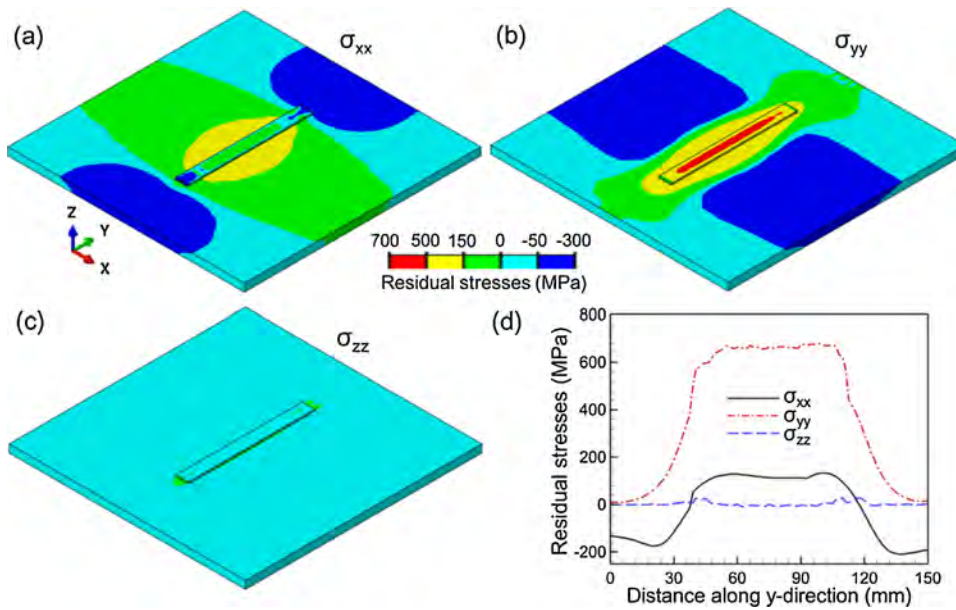


**Fig. 3.** Residual stresses of the component shown in Fig. 2 along (a) x-direction,  $\sigma_{xx}$ , (b) y-direction,  $\sigma_{yy}$ , and (c) z-direction,  $\sigma_{zz}$ , for IN 718 when the deposit cools down to room temperature and the clamps are released. (d) Comparison of the three components of residual stresses along line 1. The simulation was done for 1450 W arc power, 4.5 mm/s scanning speed, 293 K substrate preheat temperature and 5 mm substrate thickness.

**Table 1**  
Ranges of raw and causative variables.

Raw variables		Causative variables	
Variable name	Range	Variable name	Range
Power, W	1200, 1450, 1700	Pool volume, mm <sup>3</sup>	2.34 ~ 301.79
Scanning speed, mm/s	3, 4.5, 6	Substrate rigidity, $\times 10^5$ N mm <sup>2</sup>	2.98 ~ 85.64
Substrate preheat temperature, K	293, 450, 600	Difference between solidus and preheat temperatures, K	933 ~ 1365
Substrate thickness, mm	5, 10, 15	Heat input, J/mm	200 ~ 566.67
Yield stress at room temperature, MPa	577 ~ 937	Stress generated per unit temperature change, MPa /K	2.66 ~ 4.19
Expansion coefficient, $\times 10^{-5}$ K <sup>-1</sup>	1.31 ~ 2.19		
Thermal diffusivity, mm <sup>2</sup> /s	2.50 ~ 3.72		
Young's modulus, MPa	191 ~ 203		

ANN and RF [33]. The software package, instruction manuals, libraries and sample cases for “Sci-kit learn” are freely available on the website <https://scikit-learn.org/stable/>.

### 3. Results and discussions

#### 3.1. Validation of the thermomechanical model

Since the reliability of the results from machine learning depends on the accuracy of the residual stresses calculated using the thermo-mechanical model, the model outputs are rigorously tested using independent experimental data. Fig. 4 shows fair agreements between the calculated residual stresses using the thermomechanical model and the corresponding experimentally measured [34] stresses for a single track WAAM deposit of carbon steel (S235JR). The reasons for the slight mismatch between the computed residual stresses and the measured stress values may be due to the measurement error in the hole drilling method and the assumptions made in the thermomechanical model. The agreement gives us confidence that the residual stresses calculated using the thermomechanical model can be used for machine learning.

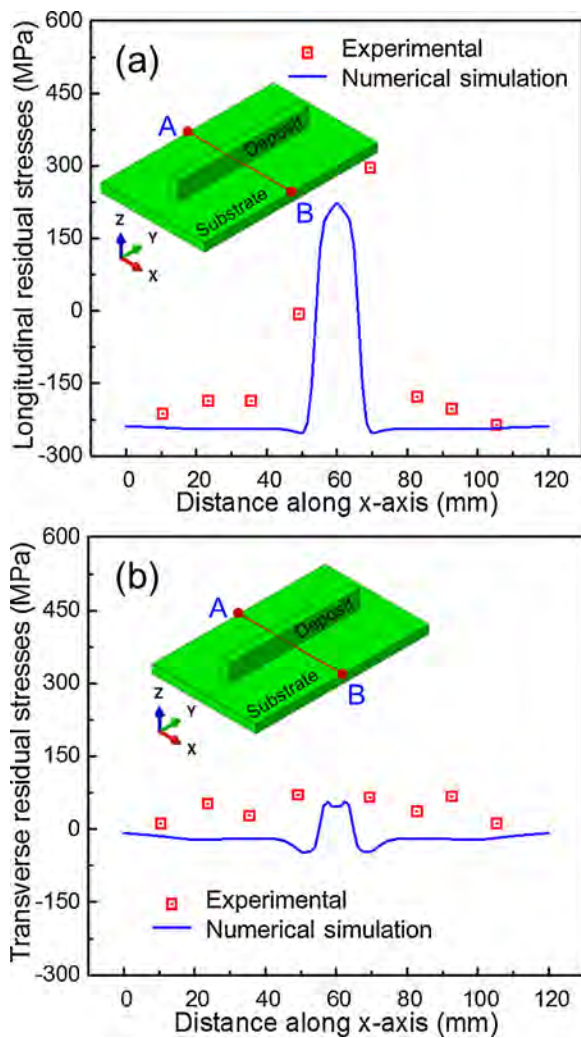


**Fig. 4.** Comparison between the experimentally measured [34] and numerically computed (a) longitudinal (along  $y$ -direction,  $\sigma_{yy}$ ) and (b) transverse (along  $x$ -direction,  $\sigma_{xx}$ ) residual stress profiles along the line AB which is at the mid-length of a single track carbon steel deposit. The line AB is on the top surface of the substrate. The processing conditions for these simulations are available in the corresponding literature [34]. Error bars for the experimental data are not reported in the original paper [34].

### 3.2. Hierarchy of raw process variables

As described in Section 2.2, a database for ML is generated by varying four WAAM variables, arc power, scanning speed, substrate thickness and preheat temperature, because these four parameters significantly affect the residual stresses. For example, Figs. 5 (a), (b), (c) and (d) show that the longitudinal residual stresses during WAAM of an IN 718 component vary significantly with arc power, scanning speed, substrate thickness and preheat temperature, respectively. Both increases in arc power and decreases in scanning speed result in a larger molten pool that shrinks more during solidification [1]. The shrinkage generates high tensile stress near the substrate-deposit interface. The thicker substrate has more rigidity that can restrict the deformation of the component and accumulate high residual stresses as shown in Fig. 5 (c). Residual stresses usually develop during cooling until the entire component cools down to a constant temperature [4]. With higher preheat temperature, the difference between the solidus temperature of alloy and the preheat temperature is smaller and, the residual stresses are also smaller. Thus, residual stresses decrease with an increase in preheat temperature as shown in Fig. 5 (d).

The aforementioned variations in residual stresses for different

process conditions and alloys generate a large dataset that is used to train and test ANN and RF as described in Section 2. In practice, two metrics are used to evaluate the performance of ANN and RF models, mean absolute error (MAE) [19] and correlation coefficient (R2) score [35]. MAE represents the mean absolute difference between the predicted stress values by ML and the stress values calculated by the thermomechanical model. A small MAE is desirable for a good ML model. The R2 score quantifies the deviation of data from their mean value and a score of 1 indicates that all predicted stress values by ML exactly match with that calculated using the thermomechanical model. Fig. 6 shows the comparison between predicted residual stresses by both ANN and RF and the calculated residual stresses by the thermomechanical model. The figures show that all data points for training and testing datasets of both ML algorithms are close to the diagonal line, indicating the predicted stress values by ML agree well with the calculated stress values by the model. These validation results indicate that both ANN and RF can be used for predicting the hierarchical influence of variables with good accuracy. ANN performs slightly better than RF with better performance metrics values (lower MAE and higher R2 score). This is mainly because ANN is good at solving complicated multi-scale multi-physics mathematical models and capturing the complex relationship between inputs and outputs [19].

Running the validated ANN to generate process maps of residual stresses for different combinations of arc power, scanning speed, substrate thickness and preheat temperature is a time-efficient way since it precludes the necessity of time-consuming thermomechanical simulations. Fig. 7 shows the process maps of longitudinal residual stresses for different combinations of the four process parameters for three alloys. Fig. 7 (a–c) show that high arc power and slow scanning speed increase residual stresses for all three alloys, which is consistent with the trends shown in Fig. 5 (a–b). Also, Fig. 7 (d–f) show that thicker substrate and low preheat temperature are favorable conditions for accumulating high residual stresses, which is also consistent with the trends shown in Fig. 5 (c–d). Fig. 7 (g–i) also shows that high arc power and low preheat temperature are the ideal conditions for high stress accumulation. In addition, all three alloys exhibit the same trend of residual stresses for the four process parameters. High residual stresses may cause thermo-mechanical defects such as delamination in WAAM components [1,2,36]. Delamination is likely to occur when the longitudinal residual stress value is higher than the room temperature yield strength and close to the ultimate tensile strength [1]. Therefore, it is assumed that a component is prone to delamination if the longitudinal residual stress is higher than the average value of yield strength and ultimate tensile strength of the alloy at room temperature. The regions of the process maps in Fig. 7 where delamination is likely to occur are indicated in orange as the background color. It is evident that for the same range of process conditions, the three alloys have different regions of susceptibility to delamination because of the differences in their thermo-physical and mechanical properties.

The process maps in Fig. 7 obtained using ANN can be used to evaluate the relative sensitivity of the four process parameters on residual stresses. Fig. 8 shows the process maps for IN 718, as an example, where the four variables are normalized to the same scale of 0–1 for comparison. Normalization is done by using the min-max normalization method [37] where a variable  $V$  is normalized to  $V^*$  as,  $V^* = (V - V_{min}) / (V_{max} - V_{min})$ .  $V_{min}$  and  $V_{max}$  are the minimum and the maximum values of the variable, respectively. By comparing the slopes of the contours for two variables in each plot in Fig. 8, the relative sensitivity of the variables to residual stresses is evaluated. For example, in Fig. 8 (b), when the normalized preheat temperature increases from 0.06 to 0.17, the residual stress decreases from 690 MPa to 660 MPa. However, to achieve the same 30 MPa decrease in residual stress, the normalized arc power needs to decrease from 0.53 to 0.3. Therefore, substrate preheat temperature is more sensitive to residual stresses than arc power. Similarly, by comparing the relative sensitivities of variables in all four plots in Fig. 8, it can be found that the residual stresses are the

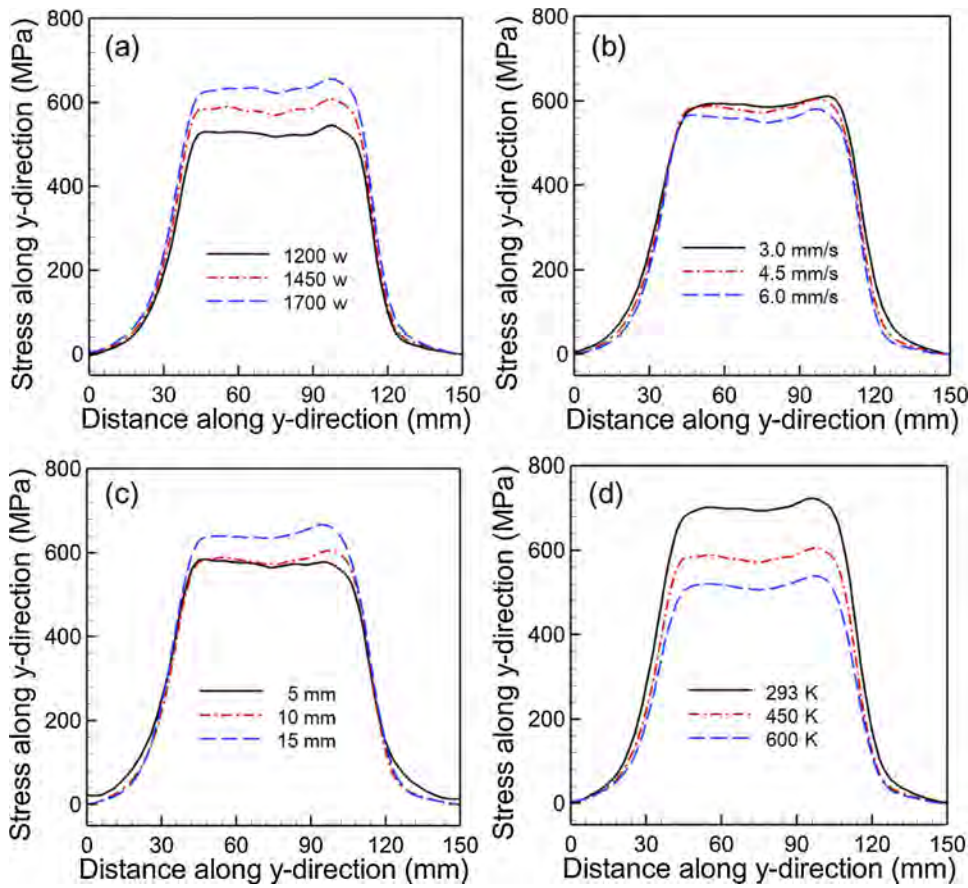


**Fig. 5.** Distribution of residual stress along y-direction (scanning direction) i.e. longitudinal residual stress along line 1 (indicated in Fig. 2) for IN 718 for different (a) arc power, (b) scanning speed, (c) substrate thickness and (d) substrate preheat temperature. When one variable is varied, other variables are kept constant at the middle values of their range. For example, for figure (a), scanning speed of 4.5 mm/s, substrate thickness of 10 mm and substrate preheat temperature of 450 K are used.

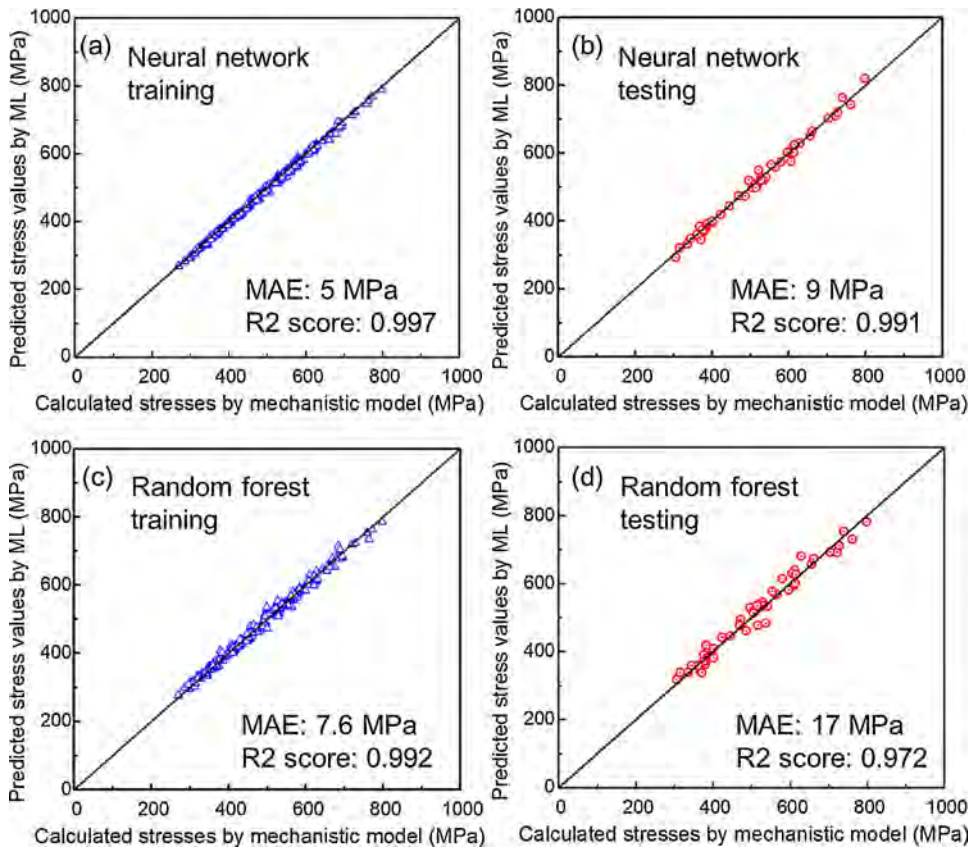


**Fig. 6.** Comparison of output stress values: (a) training dataset and (b) testing dataset calculated by thermomechanical model with corresponding stress values predicted by neural network model with raw variables in WAAM, (c) training dataset and (d) testing dataset calculated by thermomechanical model with corresponding stress values predicted by random forest model with raw variables in WAAM. The diagonal lines in each plot represent calculated stress values match exactly with the predicted values by ML. The training data and testing data comprise 194 and 49 datasets, respectively. MAE in the plot represents the mean absolute error of predicted stress values by ML and the stresses values calculated by thermomechanical model. R2 score is a statistical measure of how close the data are to the diagonal line. R2 score is always between 0 and 1. In general, the closer the R2 score is to 1, the better the model fits the data.

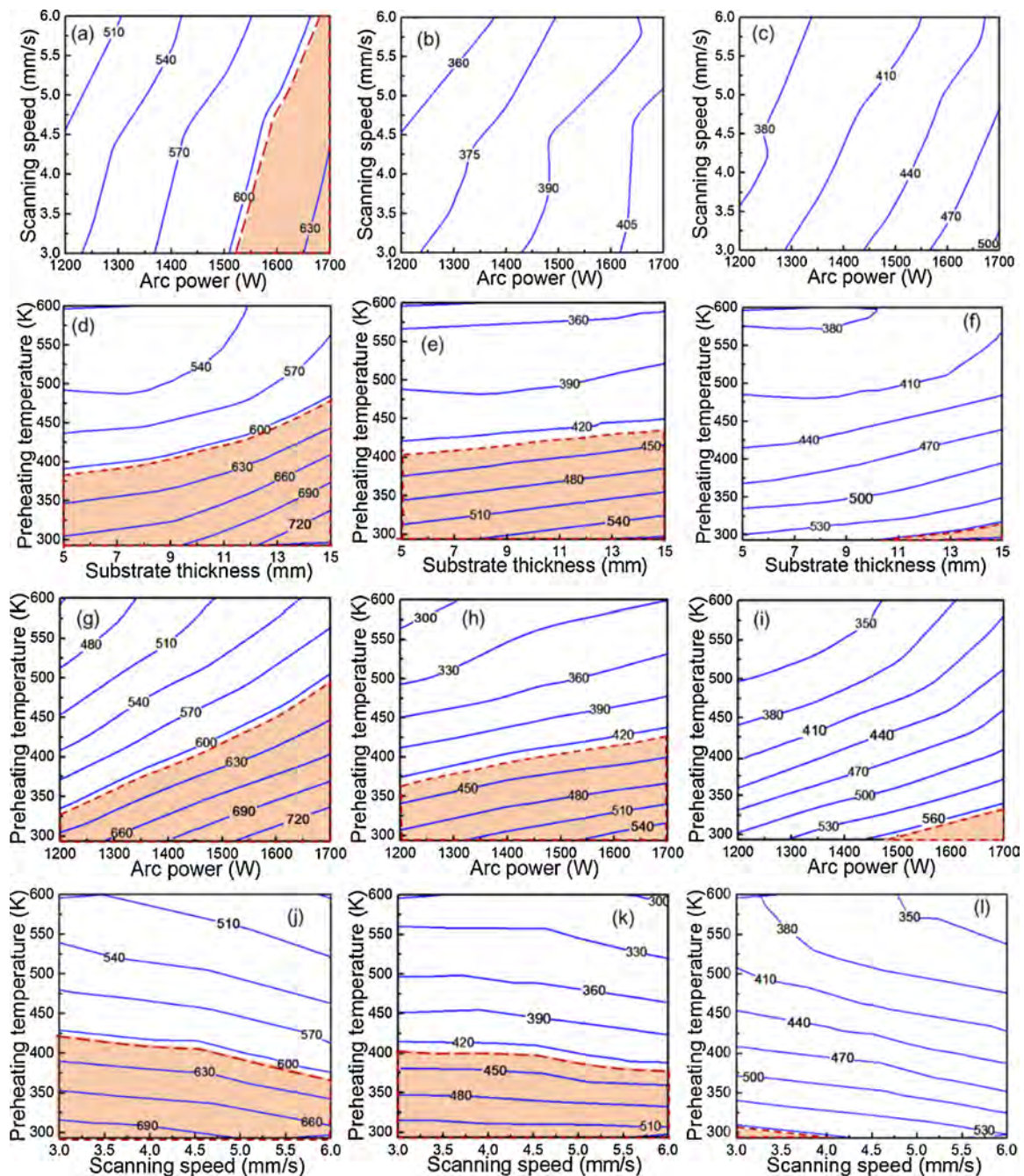


**Fig. 7.** Process maps showing longitudinal residual stress (MPa) contours computed using the ANN model for WAAM of (a) IN 718, (b) SS 316 and (c) 800H for different combinations of arc power and scanning speed, for (d) IN 718, (e) SS 316 and (f) 800H for different combination of substrate thickness and substrate preheat temperature, for (g) IN 718, (h) SS 316 and (i) 800H for different combinations of arc power and substrate preheat temperature, for (j) IN 718, (k) SS 316 and (l) 800H for different combinations of scanning speed and substrate preheat temperature. For a particular process map, when two variables are varied, other parameters are kept constant at the middle values of their range. The processing conditions that may result in delamination are indicated by orange color in each process maps. The delamination criteria used in this work for IN 718, SS 316 and 800H is 604.5 MPa, 430.5 MPa, 561.5 MPa, respectively.

most sensitive to the substrate preheat temperature, followed by the arc power and substrate thickness. Although both arc power and scanning speed equally contribute to the heat input to the system, the scanning speed has a lower influence on residual stresses than arc power. This is primarily because the effect of low heat input on residual stresses at a fast scanning speed is masked by the low exposure time due to rapid scanning. Therefore, the effect of heat input on residual stresses is largely controlled by the variations in arc power which make arc power more important than scanning speed.

The hierarchical importance of the process variables that are

obtained by analyzing their impact on residual stresses from the process maps in Fig. 8, can also be achieved by using RF. In RF, variables are ranked based on feature importance that evaluates the importance of input variables in controlling the output [32]. Fig. 9 shows that the ranking of the four process parameters identified by RF is the same as what is obtained from the ANN in Fig. 8. In addition, four alloy properties e.g. yield stress, Young's modulus, coefficient of thermal expansion/contraction and thermal diffusivity are also found to be important in controlling residual stresses in WAAM.

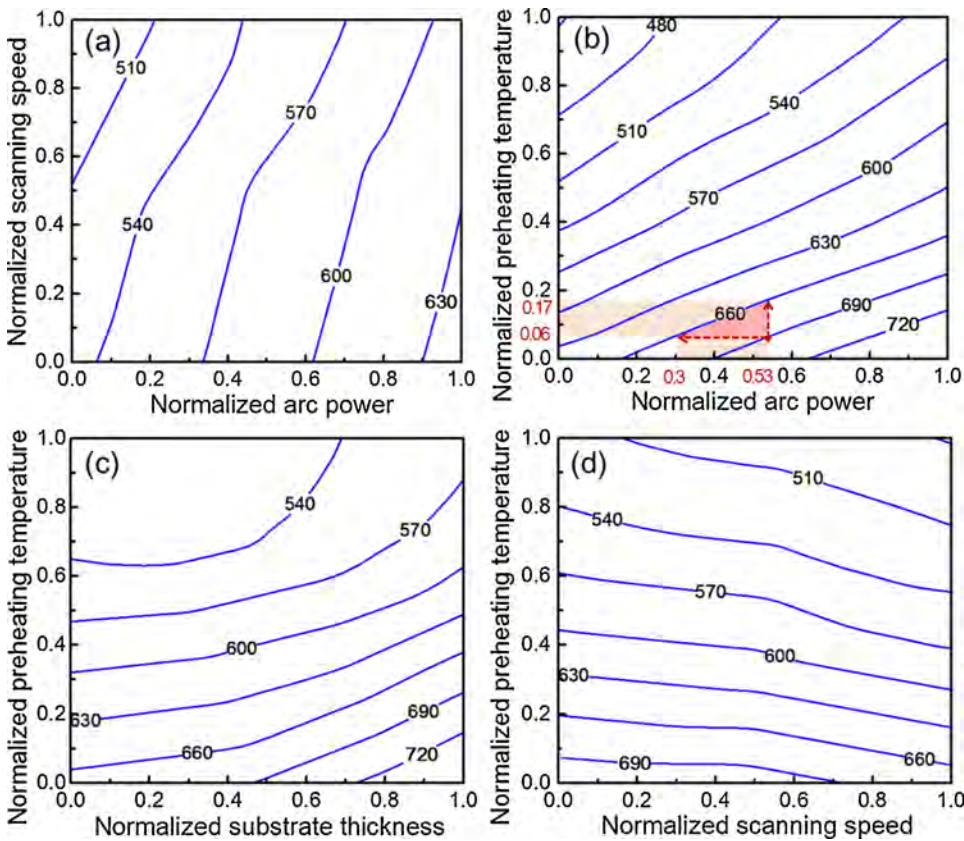


Fig. 8. Process maps showing longitudinal residual stress (MPa) contours computed using the ANN model for WAAM of IN 718 for different combinations of (a) arc power and scanning speed, (b) arc power and substrate preheat temperature, (c) substrate thickness and substrate preheat temperature and (d) scanning speed and substrate preheat temperature. For a particular process map, when two variables are varied, other parameters are kept constant at the middle values of their range.

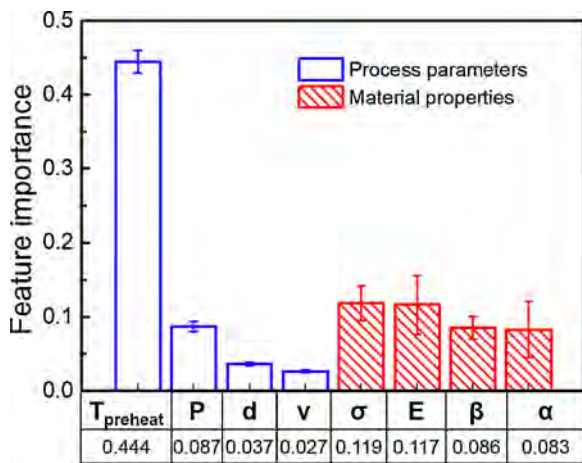


Fig. 9. Feature importance of the four WAAM parameters and alloy properties calculated by the random forest model.  $T_{preheat}$  is substrate preheat temperature,  $P$  is arc power,  $d$  is substrate thickness and  $v$  is scanning speed.  $\sigma$ ,  $E$ ,  $\beta$  and  $\alpha$  refer to yield stress at room temperature, Young's modulus, expansion coefficient and thermal diffusivity at room temperature, respectively. The corresponding feature importance values are indicated below the variables in the figure. The feature importance of the variables is calculated every time for the five-times randomly selected 194 datasets from 243 datasets. The final feature importance values of variables are averaged by the results from the five times, and the standard deviation is shown as an error bar. Process parameters windows for which the feature importance of different variables are calculated in this figure are given in Table 1.

### 3.3. Hierarchy of thermomechanical variables

The hierarchical importance shown in Figs. 7–9 is for raw process parameters in WAAM. However, the evolution of residual stresses in WAAM is a complex thermomechanical phenomenon that involves

multiple simultaneously occurring physical processes [1]. Therefore, complex variables that represent both thermal and mechanical behaviors of the system during WAAM can be better representatives of the evolution of residual stresses compared to the raw process variables. In WAAM, residual stresses develop depending on the transient variation of temperature field [4]. Fig. 10 (a) shows the temperature and corresponding stress variations with time at point A (in Fig. 2) for an IN 718 deposit. As the arc heat source approaches point A, the temperature at that location increases. The expansion of the material at that location due to a rise in temperature is restricted by the surrounding cold material which results in compressive stress at point A. When the heat source moves away from the location, the temperature at point A decreases. The stresses primarily develop during the cooling from the solidus to preheat temperature (Fig. 10 (a)) as the complete build is expected to cool down uniformly from the preheat to room temperature without evolution of any significant additional stresses. Therefore, the difference between solidus and preheat temperature is an important factor controlling the residual stresses. Fig. 10 (b) shows that the longitudinal residual stress at point A (in Fig. 2) for three alloys increases with the difference between solidus and preheat temperature. In addition, it should be noted that for the same temperature difference, the residual stresses vary significantly for different alloys. Mechanical properties of alloys such as co-efficient of thermal expansion / contraction and Young's modulus and therefore their product which is known as the stress developed per unit temperature change is also an important factor. Fig. 10 (c) shows that the three alloys accumulate different stresses values due to the differences in their mechanical properties.

Transient temperature variation in Fig. 10 (a) which is responsible for the evolution of residual stresses, is primarily governed by the heat input per unit length of the deposit (arc power/scanning speed) [38]. High heat input results in both large molten pool and high peak temperature, both of which are favorable for the accumulation of more residual stresses as shown in Fig. 10 (d). In addition to the thermal

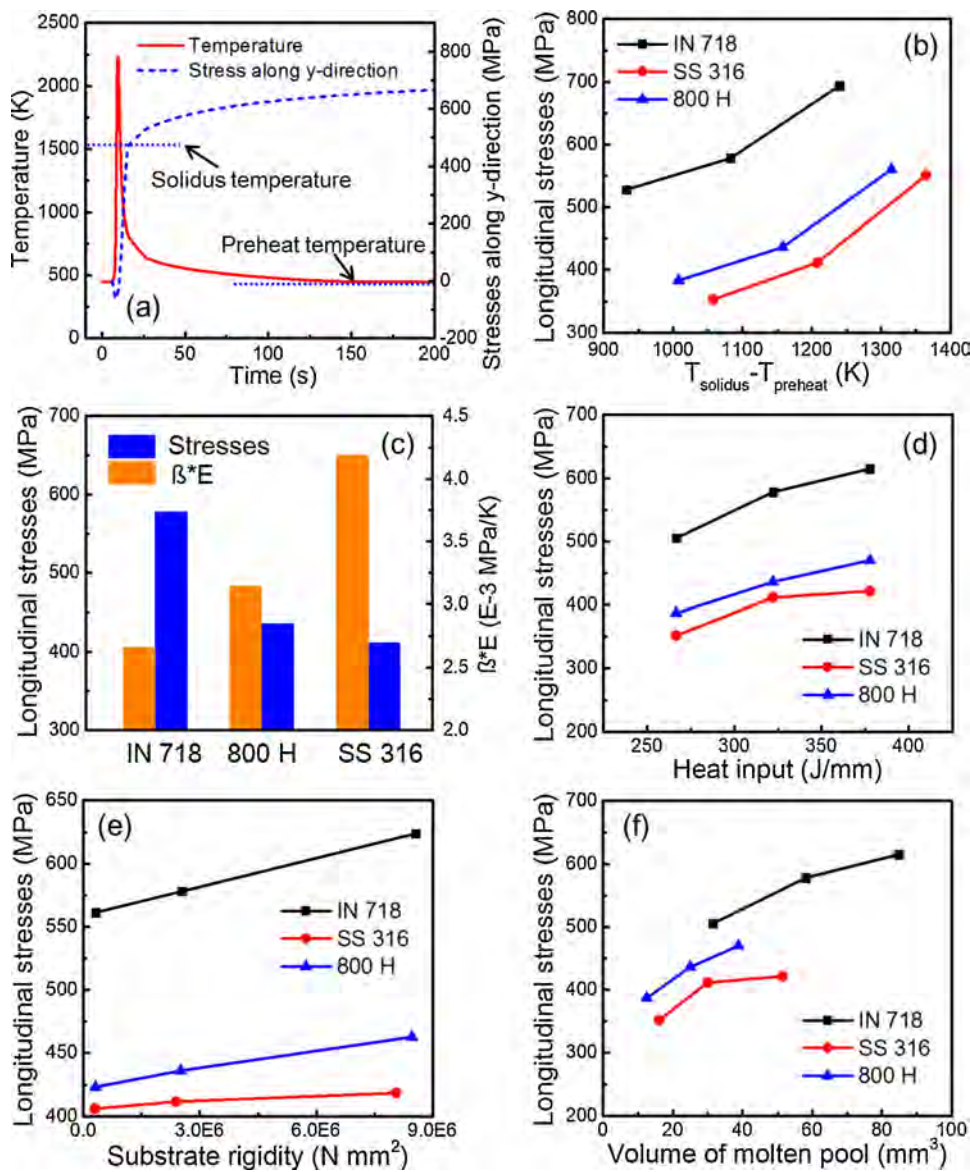


Fig. 10. (a) Temperature and longitudinal stress variations with time at point A (in Fig. 2) for an IN 718 deposit. All processing parameters are selected as the mid values of their ranges in Table 1. Effects of (b) difference between solidus and preheat temperatures, (c) stress generated per unit temperature change, (d) heat input, (e) substrate rigidity and (f) pool volume on longitudinal stresses at point A (in Fig. 2) for three alloys. Pool volumes are calculated at the mid length of the deposit. Stresses are calculated with substrate preheat temperature of 293 K, 450 K and 600 K individually for each material in (b). Stresses are calculated with arc power of 1200 W, 1450 W and 1700 W individually for each material in (d) and (f). Stresses are calculated with substrate thickness of 5 mm, 10 mm and 15 mm individually for each material in (e).

effect, the evolution of residual stresses in WAAM also depends on the mechanical behavior of the system such as rigidity of the substrate. The rigidity of the substrate is defined by the product of Young's modulus to the moment of inertia [1]. The rigid substrate has more capability to restrict the shrinkage during the solidification and cooling that results in high residual stresses as shown in Fig. 10 (e). Although most of the stresses develop during cooling from solidus to preheat temperature as shown in Fig. 10 (a), localized solidification shrinkage of the molten pool also partially contributes to the development of residual stresses. Therefore, the volume of the molten pool that can quantitatively indicate the solidification shrinkage is considered as a contributing factor to the residual stresses. Fig. 10 (f) shows that a large molten pool shrinks more during solidification and results in high residual stresses.

From the aforementioned discussions, it is evident that the five thermomechanical variables, the difference between solidus and preheat temperatures, the stress generated per unit temperature change, heat input, substrate rigidity, and pool volume are important for residual stresses in WAAM. These variables are calculated for different process conditions and alloys to generate a large dataset that is used to train and test ANN and RF. Two metrics, mean absolute error (MAE) [19] and correlation coefficient (R2) score [35] are used to evaluate the performance of ANN and RF models, same as Fig. 6. Fig. 11 shows the comparison between predicted residual stresses by both ANN and RF

and the calculated residual stresses by the thermomechanical model. The figures show that all data points for training and testing datasets of both ML algorithms are close to the diagonal line, indicating the predicted stress values by ML agree well with the calculated stress values by the model. This agreement also verifies the effectiveness of the selection of the five thermomechanical variables, based on which the residual stresses can be predicted accurately.

Unlike raw process parameters, for which both ANN and RF are used for predicting hierarchical influence, only RF is used to rank the five complex thermomechanical variables. Since the five complex thermomechanical variables are inherently connected, it is not possible to vary two variables independently while other variables are kept constant. For example, an increase in arc power results in higher heat input per unit length of the deposit as well as larger pool volume both of which are causative variables responsible for residual stress accumulation. Therefore, the ranking of variables by analyzing the sensitivity of residual stresses to these variables based on process maps generated by ANN is not applicable to evaluate the hierarchical influence of five thermomechanical variables.

Fig. 12 shows that the difference between solidus and preheat temperature is the most influential factor for residual stresses. This is primarily because most of the stresses develop during the cooling from solidus to preheat temperature as explained in Fig. 10 (a). Stress

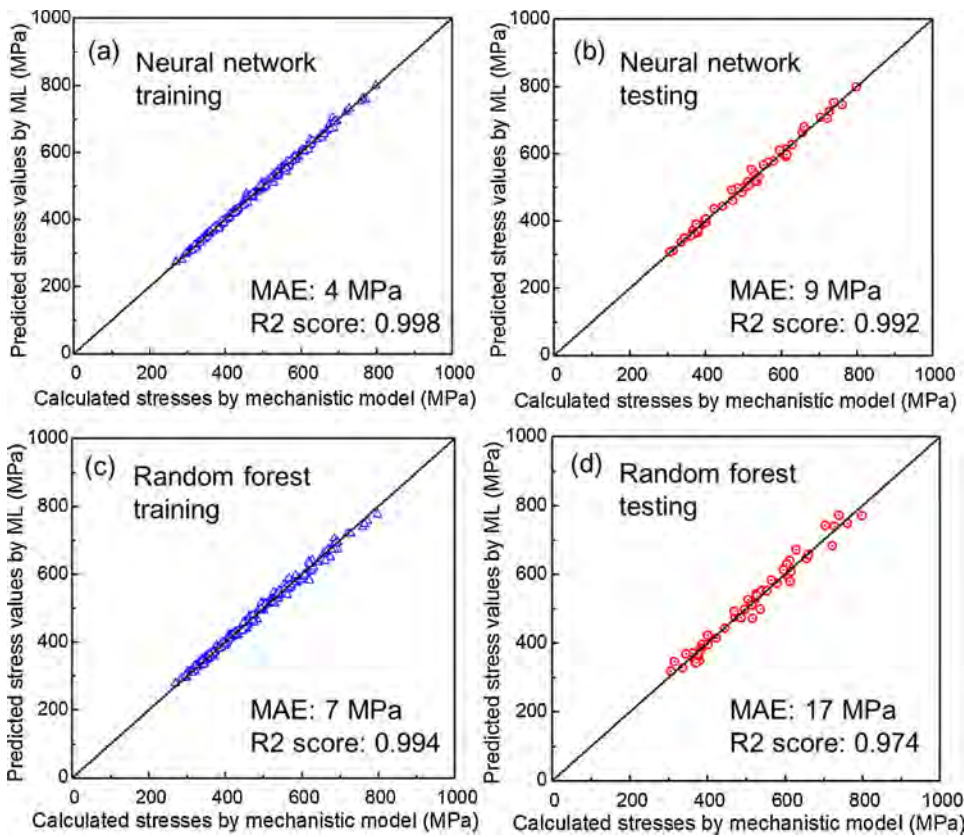


**Fig. 11.** Comparison of output stress values: (a) training dataset and (b) testing dataset calculated by thermomechanical model with corresponding stress values predicted by neural network model with five complex thermomechanical variables in WAAM, (c) training dataset and (d) testing dataset calculated by thermomechanical model with corresponding stress values predicted by random forest model with five complex thermomechanical variables in WAAM. The diagonal lines in each plot represent calculated stress values match exactly with the predicted values by ML. The training data and testing data comprise 194 and 49 datasets, respectively. MAE in the plot represents the mean absolute error of predicted stress values by ML and the stresses values calculated by thermomechanical model. R2 score is a statistical measure of how close the data are to the diagonal line. R2 score is always between 0 and 1. In general, the closer the R2 score is to 1, the better the model fits the data.

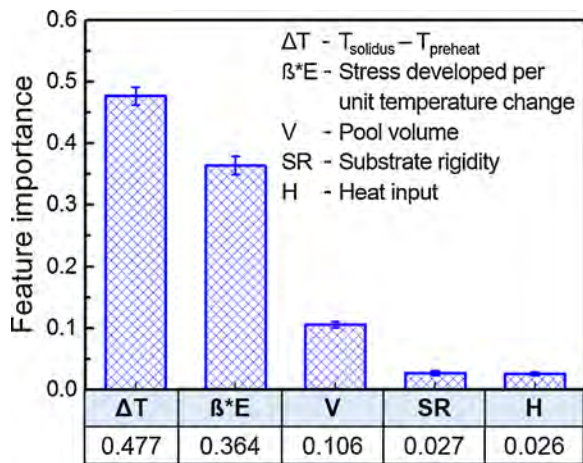


**Fig. 12.** Feature importance of the causative parameters calculated by the random forest model. The corresponding feature importance values are indicated below the variables. The feature importance of the variables is calculated every time for the five-times randomly selected 194 datasets from 243 datasets. The final feature importance values of variables are averaged by the results from the five times, and the standard deviation is shown as an error bar. The symbol  $\beta$  represents the coefficient of thermal expansion and E is the Young's Modulus. Process parameters windows for which the feature importance of different variables are calculated in this figure are given in Table 1.

generated per unit temperature change is the second most important variable primarily because the residual stresses can vary significantly for different alloys for the same processing conditions. The evolution of

residual stresses depends more on the thermomechanical behavior of the entire component compared to the localized solidification shrinkage of the molten pool. Therefore, the pool volume is less influential on residual stresses compared to the difference between solidus and pre-heat temperature as shown in Fig. 12. Residual stresses depend on the net heat content in the system, which contains both the heat input from the arc source as well as the heat from the preheating. However, the variable, heat input, represents the only heat available from the arc source. In other words, for the same heat input, residual stresses can vary largely for different preheat temperature. That makes the residual stress least sensitive to heat input.

The identification of the five complex thermomechanical variables and their hierarchical influence on residual stresses will substantially advance the scientific understanding of the role of important variables in WAAM. In addition, the hierarchical influence of the raw process parameters will guide engineers to know which variables to adjust to fabricate structurally sound and defect-free components.

#### 4. Summary and conclusions

We propose a unique combination of machine learning and a well-tested thermomechanical model to identify the most important variables and their hierarchical influence on residual stresses and delamination. Two hundred and forty-three data sets for three commonly used alloys, IN 718, SS 316 and 800H are generated using a well-tested thermomechanical model and are used in random forest and neural network-based machine learning. Below are the specific findings:

- (1) Both random forest and neural network algorithms have been found to predict residual stresses and delamination in WAAM with more than 97

- % accuracy. Besides, both algorithms provide the same hierarchical influence of WAAM process variables on stresses where preheat temperature is found to be the most important followed by arc power, substrate thickness and scanning speed in controlling stresses.
- (2) Using both neural network and random forest, we identified five complex thermomechanical variables that represent the complex mechanisms of evolution of residual stresses better than the individual WAAM process variables. They include three thermal variables, the difference between solidus and preheat temperature, liquid pool volume, heat input, and mechanical variables, substrate rigidity, and the product of elastic modulus and coefficient of thermal expansion.
  - (3) Among the five thermomechanical variables, the difference between the solidus and preheat temperature was found to be the most important parameter. This is mainly because residual stresses originate during cooling from the solidus to preheat temperature. As the temperature further decreases from the preheat to room temperature, the whole component cools down uniformly and no significant additional stresses develop.
  - (4) The product of elastic modulus and the coefficient of thermal expansion that represents the stress developed per unit change in temperature and volume of the molten pool are the second and third most influential variables that affect residual stresses. For the same range of cooling, residual stresses vary significantly depending on the material property, which makes residual stresses highly sensitive to stress developed per unit change in temperature. Residual stresses depend on the thermomechanical behavior of the

entire component and not only on the localized shrinkage of the molten pool volume. The pool volume was not as influential as the other variables on residual stresses.

- (5) Although the thermophysical properties of three alloys, IN 718, SS 316 and 800H, vary within the same range of process parameters, the variation of residual stresses shows a similar trend. However, magnitudes of stresses are different for three alloys due to the differences in their thermophysical and mechanical properties. These differences in stress values make their susceptibility to delamination different under the same processing conditions.

#### CRedit authorship contribution statement

**Q. Wu:** Methodology, Writing - original draft, Software, Validation.  
**T. Mukherjee:** Conceptualization, Software, Investigation, Writing - original draft.  
**A. De:** Investigation, Writing - review & editing.  
**T. DebRoy:** Conceptualization, Supervision, Writing - review & editing.

#### Declaration of Competing Interest

None.

#### Acknowledgement

Q. Wu acknowledges the support of the China Scholarship Council [grant number 201806030114].

#### Appendix A. Does the hierarchy depend on the absolute values of residual stresses?

In wire-arc additive manufacturing, generally, components are made by depositing multiple layers [4]. Residual stress values in the component vary with the progress of the multi-layer deposition process [4]. Fig. A1 shows that the longitudinal residual stresses change with the deposition of different layers along the build direction [39]. This is primarily due to the repeated thermal cycles experienced by the component during layer-by-layer deposition [39]. Therefore, the residual stress values of a single layer may vary from that in a multi-layer deposit. It is important to evaluate if the values of the first layer can be reliably used to determine the hierarchy of variables that affect the residual stresses. We do so using various approaches.

First, it is well-established in the machine learning literature that the variables need to be non-dimensionalized [40–42] on a scale generally between 0 and 1 for obtaining their hierarchy. This is because different variables have diverse order of magnitudes of values. In our case, all variables including the residual stress are normalized on a scale between 0 and 1. Therefore, the hierarchy depends on the trends and not absolute values of the residual stress which vary with the deposition of different layers.

Second, it can be shown mathematically that the hierarchy of the input variables does not depend on the magnitude of the output variable (residual stresses). Consider the variation of the output variable residual stress ( $\sigma$ ) as functions of two independent variables  $X$  and  $Y$ . For a particular value of  $\sigma$ , if  $X$  has a higher influence on residual stress than  $Y$ , then the following expression is true:

$$\left| \frac{\partial \sigma}{\partial X} \right| / \left| \frac{\partial \sigma}{\partial Y} \right| > 1 \quad (\text{A1})$$

If the value of residual stress in a different layer is higher by  $\Delta\sigma$ , such that:

$$\frac{\partial(\Delta\sigma)}{\partial X} = 0 \text{ and } \frac{\partial(\Delta\sigma)}{\partial Y} = 0 \quad (\text{A2})$$

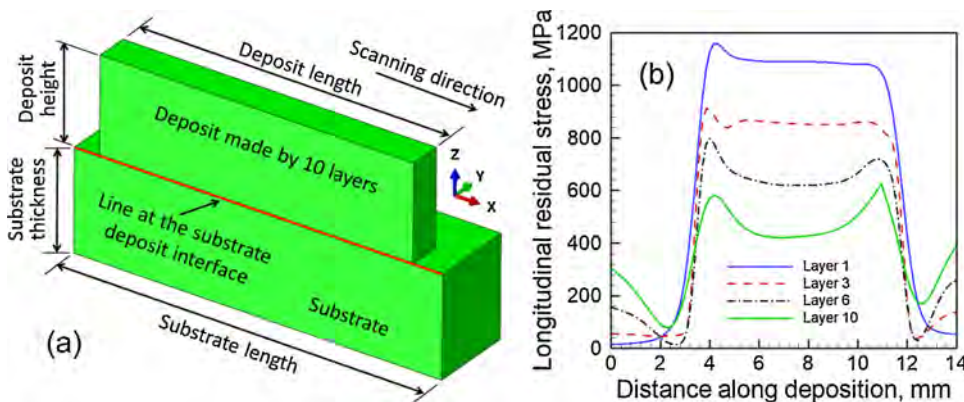


**Fig. A1.** (a) A schematic diagram of the solution domain for the calculations showing the line at the substrate deposit interface along which the stresses are plotted [39]. Calculations are done for half of the build. This reduces the time necessary for the calculations and the computer memory requirements for the analysis. (b) Residual stresses [39] after depositing various layers along the line shown in figure (a).

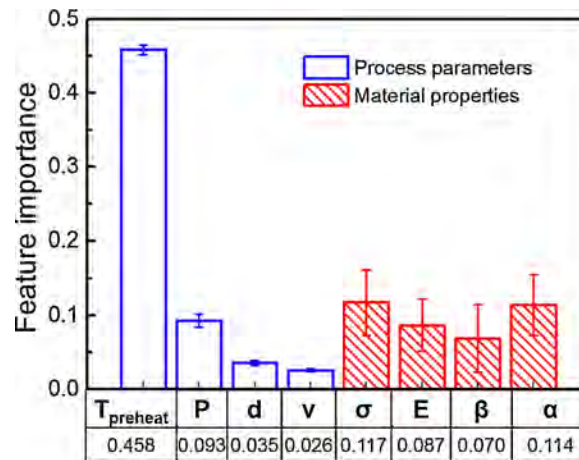


**Fig. A2.** Feature importance of the four WAAM parameters and alloy properties calculated by the random forest model using the new dataset explained in the appendix.  $T_{preheat}$  is substrate preheat temperature,  $P$  is arc power,  $d$  is substrate thickness and  $v$  is scanning speed.  $\sigma$ ,  $E$ ,  $\beta$  and  $\alpha$  refer to yield stress at room temperature, Young's modulus, expansion coefficient and thermal diffusivity at room temperature, respectively. The corresponding feature importance values are indicated below the variables in the figure. The feature importance of the variables is calculated every time for the five-times randomly selected 194 datasets from 243 datasets. The final feature importance values of variables are averaged by the results from the five times, and the standard deviation is shown as an error bar. Process parameters windows for which the feature importance of different variables is calculated in this figure are given in Table 1.

The same hierarchy, i.e.,  $X$  is more influential than  $Y$  would be valid as can be observed from the following expression.

$$\left| \frac{\partial(\sigma + \Delta\sigma)}{\partial X} \right| / \left| \frac{\partial(\sigma + \Delta\sigma)}{\partial Y} \right| > 1 \quad (\text{A3})$$

Since Eq. (A3) is the same as Eq. (A1), the hierarchy of variables  $X$  and  $Y$  are unaffected by the absolute values but depends on the trends in variations. It is well-known in the additive manufacturing literature [12] that the trends in the variations of residual stresses with variables such as power, speed, substrate thickness, preheat temperature do not change with the number of layers deposited. Therefore, the hierarchy of variables computed using the data of a single layer deposit is also valid for multi-layer deposits.

Third, we have repeated the calculations presented in this paper with two layers of deposition and evaluated the hierarchy using the same procedure. In other words, we have calculated the residual stresses at the substrate deposit interface after depositing the second layer for the IN 718 deposit using 1450 W power, 4.5 mm/s scanning speed, 10 mm substrate thickness, and 450 K preheat temperature. The maximum stress value is about 0.75 times the maximum value for the single layer deposit. Following the trend, we have made a new dataset with 243 data points and calculated the hierarchy of raw variables and alloy properties which is shown in Fig. A2. The hierarchy of variables shown in the figure is the same as what is provided in Fig. 9 for the single layer deposit. The hierarchy remained the same as that for a single layer deposit. In addition, the calculation of hierarchy using the first layer deposition is computationally more efficient since the residual stress calculations are computationally intensive.

## Appendix B. Supplementary data

Supplementary material related to this article can be found, in the online version, at doi:<https://doi.org/10.1016/j.addma.2020.101355>.

## References

- [1] T. DebRoy, H.L. Wei, J.S. Zuback, T. Mukherjee, J.W. Elmer, J.O. Milewski, et al., Additive manufacturing of metallic components - process, structure and properties, *Prog. Mater. Sci.* 92 (2018) 112–224.
- [2] T. DebRoy, T. Mukherjee, J.O. Milewski, J.W. Elmer, B. Ribic, J.J. Blecher, et al., Scientific, technological and economic issues in metal printing and their solutions, *Nat. Mater.* 18 (2019) 1026–1032.
- [3] W. Ou, T. Mukherjee, G.L. Knapp, Y. Wei, T. DebRoy, Fusion zone geometries, cooling rates and solidification parameters during wire arc additive manufacturing, *Int. J. Heat Mass Transf.* 127 (2018) 1084–1094.
- [4] Q. Wu, T. Mukherjee, C. Liu, J. Lu, T. DebRoy, Residual stresses and distortion in the patterned printing of titanium and nickel alloys, *Addit. Manuf.* (2019) 100808.
- [5] J.D. Roehling, W.L. Smith, T.T. Roehling, B. Vrancken, G.M. Guss, J.T. McKeown, et al., Reducing residual stress by selective large-area diode surface heating during laser powder bed fusion additive manufacturing, *Addit. Manuf.* 28 (2019) 228–235.
- [6] C. Cunningham, J. Flynn, A. Shokrani, V. Dhokia, S. Newman, Invited review article: strategies and processes for high quality wire arc additive manufacturing, *Addit. Manuf.* (2018).
- [7] T. Mukherjee, V. Manvatkar, A. De, T. Debroy, Mitigation of thermal distortion during additive manufacturing, *Scr. Mater.* 127 (2017) 79–83.
- [8] J. Xiong, Y. Lei, R. Li, Finite element analysis and experimental validation of thermal behavior for thin-walled parts in GMAW-based additive manufacturing with various substrate preheating temperatures, *Appl. Therm. Eng.* (2017) 126.
- [9] M. Alimardani, E. Toyserkani, J.P. Huissoon, C.P. Paul, On the delamination and crack formation in a thin wall fabricated using laser solid freeform fabrication process: an experimental–numerical investigation, *Opt. Lasers Eng.* 47 (2009) 1160–1168.
- [10] J.L. Bartlett, X. Li, An overview of residual stresses in metal powder bed fusion, *Addit. Manuf.* (2019).
- [11] Y. Liu, Y. Yang, D. Wang, A study on the residual stress during selective laser melting (SLM) of metallic powder, *Int. J. Adv. Manuf. Technol.* 87 (2016) 647–656.
- [12] P. Merceles, J.P. Kruth, Residual stresses in selective laser sintering and selective laser melting, *Rapid Prototyp. J.* 12 (2006) 254–265.
- [13] J. Mathew, J. Griffin, M. Alamaniotis, S. Kanarachos, M. Fitzpatrick, Prediction of welding residual stresses using machine learning: comparison between neural networks and neuro-fuzzy systems, *Appl. Soft Comput.* 70 (2018) 131–146.
- [14] Y.D. Koo, K.H. Yoo, G.N. Man, Estimation of residual stress in welding of dissimilar metals at nuclear power plants using cascaded support vector regression, *Nucl. Eng. Technol.* 49 (2017) S173857331630345X.
- [15] N. Ansaripour, A. Heidari, S.A. Eftekhari, Multi-objective optimization of residual

- stresses and distortion in submerged arc welding process using Genetic Algorithm and Harmony search, Proc. Inst. Mech. Eng. Part C J. Mech. Eng. Sci. (2019) 0954406219885977.
- [16] J.E.R. Dhas, S. Kumaran, Evolutionary fuzzy SVR modeling of weld residual stress, Appl. Soft Comput. 42 (2016) 423–430.
- [17] J.E.R. Dhas, S. Kumaran, Neuro evolutionary model for weld residual stress prediction, Appl. Soft Comput. 14 (2014) 461–468.
- [18] M. Alamaniotis, J. Mathew, A. Chroneos, M.E. Fitzpatrick, L.H. Tsoukalas, Probabilistic kernel machines for predictive monitoring of weld residual stress in energy systems, Eng. Appl. Artif. Intell. 71 (2018) 138–154.
- [19] X. Qi, G. Chen, Y. Li, G.X. Chen, C. Li, Applying neural-network-Based machine learning to additive manufacturing: current Applications, challenges, and future perspectives, Engineering (2019).
- [20] Y. LeCun, Y. Bengio, G. Hinton, Deep learning. nature 521 (2015) 436.
- [21] V. Svetnik, A. Liaw, C. Tong, J.C. Culberson, R.P. Sheridan, B.P. Feuston, Random forest: a classification and regression tool for compound classification and QSAR modeling, J. Chem. Inf. Comput. Sci. 43 (2003) 1947–1958.
- [22] K. Khan, A. De, Modelling of selective laser melting process with adaptive re-meshing, Sci. Technol. Weld. Join. (2019) 1–10.
- [23] T. Mukherjee, W. Zhang, T. Debroy, An improved prediction of residual stresses and distortion in additive manufacturing, Comput. Mater. Sci. 126 (2017) 360–372.
- [24] Abaqus Documentation, Version 6.14, Dassault Systems, 2015.
- [25] F. Martina, M. Roy, B. Szost, S. Terzi, P.A. Colegrove, S.W. Williams, et al., Residual stress of as-deposited and rolled wire + arc additive manufacturing Ti–6Al–4V components, Mater. Sci. Technol. 32 (2016) 1439–1448.
- [26] J. Ding, P. Colegrove, J. Mehnert, S. Ganguly, P.S. Almeida, F. Wang, et al., Thermo-mechanical analysis of Wire and Arc Additive Layer Manufacturing process on large multi-layer parts, Comput. Mater. Sci. 50 (2011) 3315–3322.
- [27] H.D. Beale, H.B. Demuth, M. Hagan, Neural network design, Pws, Boston (1996).
- [28] P. Liashchynskiy, P. Liashchynskiy, Grid search, random search, genetic algorithm: a big comparison for NAS, arXiv preprint arXiv 191206059 (2019).
- [29] X. Glorot, A. Bordes, Y. Bengio, Deep sparse rectifier neural networks, Proceedings of the fourteenth international conference on artificial intelligence and statistics (2011) 315–323.
- [30] A. Liaw, M. Wiener, Classification and regression by RandomForest, R news 2 (2002) 18–22.
- [31] L. Breiman, Random forests, Mach. Learn. 45 (2001) 5–32.
- [32] M. Sandri, P. Zuccolotto, Analysis and correction of bias in total decrease in node impurity measures for tree-based algorithms, Stat. Comput. 20 (2010) 393–407.
- [33] F. Pedregosa, G. Varoquaux, A. Gramfort, V. Michel, B. Thirion, O. Grisel, et al., Scikit-learn: machine learning in Python, J. Mach. Learn. Res. 12 (2011) 2825–2830.
- [34] H. Zhao, G. Zhang, Z. Yin, L. Wu, Three-dimensional finite element analysis of thermal stress in single-pass multi-layer weld-based rapid prototyping, J. Mater. Process. Technol. 212 (2012) 276–285.
- [35] P. Ahlgren, B. Jarneving, R. Rousseau, Requirements for a cocitation similarity measure, with special reference to Pearson's correlation coefficient, J. Am. Soc. Inf. Sci. Technol. 54 (2003) 550–560.
- [36] T. Mukherjee, T. DebRoy, Printability of 316 stainless steel, Sci. Technol. Weld. Join. (2019) 1–8.
- [37] S. Patro, K.K. Sahu, Normalization: a preprocessing stage, arXiv preprint arXiv (2015) 150306462.
- [38] T. Mukherjee, V. Manvatkar, A. De, T. Debroy, Dimensionless numbers in additive manufacturing, J. Appl. Phys. 2017 (121) (2017).
- [39] T. Mukherjee, J.S. Zuback, W. Zhang, T. DebRoy, Residual stresses and distortion in additively manufactured compositionally graded and dissimilar joints, Comput. Mater. Sci. 143 (2018) 325–337.
- [40] Y. Du, T. Mukherjee, P. Mitra, T. DebRoy, Machine learning based hierarchy of causative variables for tool failure in friction stir welding, Acta Mater. 192 (2020) 67–77.
- [41] Y. Du, T. Mukherjee, T. DebRoy, Conditions for void formation in friction stir welding from machine learning, Npj Comput. Mater. 5 (2019) 1–8.
- [42] O. Genc, A. Dag, A Bayesian network-based data analytical approach to predict velocity distribution in small streams, J. Hydroinformatics 18 (2016) 466–480.